

# FULL-SCALE MEASUREMENTS OF WELDING-INDUCED INITIAL DEFLECTIONS AND RESIDUAL STRESSES IN STEEL-STIFFENED PLATE STRUCTURES

(DOI No: 10.3940.rina.ijme.2018.a4.504)

**M S Yi**, Department of Naval Architecture and Ocean Engineering at Pusan National University; and Samsung Heavy Industries, South Korea; **C M Hyun**, Samsung Heavy Industry, South Korea; and **J K Paik**, The International Centre for Advanced Safety Studies (The Lloyd's Register Foundation Research Centre of Excellence), South Korea; and University College London, UK

## SUMMARY

Plated structures such as ships and offshore structures are constructed using welding techniques that attach support members (or stiffeners) to the plating. During this process, initial imperfections develop in the form of initial deformations (deflections or distortions) and residual stresses. These initial imperfections significantly affect the buckling and ultimate strength of these structures. Therefore, to assess the strength of welded plate structures, it is very important to predict the magnitude and pattern of welding-induced initial imperfections and their effects on buckling and ultimate strength. To determine the reliability of the prediction methods, it is desirable to validate the theoretical or numerical predictions of welding-induced initial imperfections through comparison with full-scale actual measurements. However, full-scale measurement databases are lacking, as they are costly to obtain. This study contributes to the development of a full-scale measurement database of welding-induced initial imperfections in steel-stiffened plate structures. The target structures are parts of real (full-scale) deckhouses in very large crude oil carrier class floating, production, storage and offloading unit structures. For parametric study purposes, four test structures by varying plate thickness are measured while the stiffener types and weld bead length are fixed. Modern technologies for measuring initial deformations and residual stresses are applied. The details of the measurement methods are documented for the use of other researchers and practicing engineers who want to validate their computational models for predicting welding-induced initial imperfections.

## ABBREVIATIONS

CMM Coordinate Measuring Machine  
 CPM Centimetre Per Minute  
 FCAW Flux Cored Arc Welding  
 HAZ Heat Affected Zone  
 LQ Living Quarter  
 WPS Welding Parameter Specification  
 XRD X-Ray Diffraction

## 1. INTRODUCTION

Stiffened plate structures in ships and offshore platforms (Figure 1) are formed where support members (stiffeners) are welded to plating. During this process, initial imperfections develop in the form of initial deflections (Figure 2) and residual stresses (Figure 3). The strength of welded structures is significantly affected by welding-induced initial imperfections (Paik, 2018). Thus, it is of paramount importance to accurately predict the magnitudes and patterns of such initial imperfections and their effects on the buckling and ultimate strength of these structures.

Theoretical or numerical predictions are not always entirely accurate or efficient, and it is necessary to validate them through comparison with experimental data. Tests using small-scale structure models may distort the real mechanisms, as although the welding procedure is real, the structure models are scaled down with unrealistically thin wall thickness. Therefore, it is

extremely important to have a full-scale test database to characterise the mechanisms and to reliably verify the computational models.

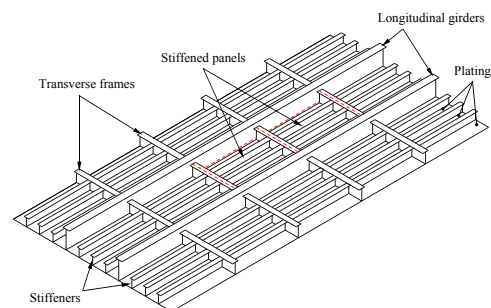


Figure 1: Stiffened plate structures (Paik, 2018)

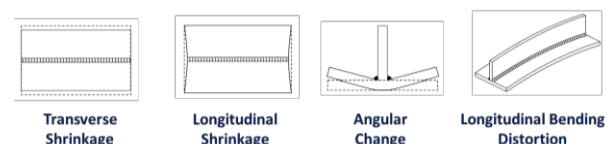


Figure 2: Pattern of welding-induced initial deflections in stiffened plate structures (Paik, 2018)

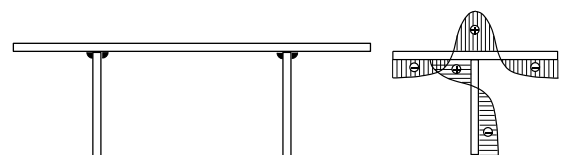


Figure 3: Pattern of welding-induced residual stresses in stiffened plate structures (Paik, 2018)

A number of previous studies have engaged in the direct measurement of welding-induced initial imperfections in steel or aluminium stiffened plate structures. For example, Masubuchi (1980), Smith et al. (1988), Ueda (1999), Paik et al. (2006), Paik (2007c, 2008), Paik et al. (2008, 2012), Vhanmane et al. (2008), Luis et al. (2009), Bruno et al. (2011), Khedmati et al. (2012) and Teresaet al. (2013) have measured the initial distortions of aluminium-plated structures; Masubuchi (1980), Smith et al. (1988), Cheng et al. (1996), Ueda (1999) and Kenno et al. (2010, 2017) have measured the residual stress of steel-plated structures; and Paik et al. (2006), Paik (2008) and Paik et al. (2008, 2012) have measured the residual stresses and softening of aluminium-plated structures. Recent studies of the effects of initial imperfections caused by welding on fatigue strength include Eggert et al. (2012) and Lillemäe et al. (2017), who measured the residual stress of steel-plated structures. Other relevant studies are Khan et al. (2011), Gannon et al. (2012a, 2012b, 2015), Farajkhah et al. (2016) and Chen et al. (2018).

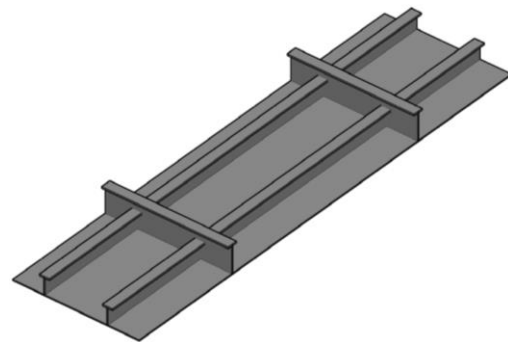
The existing test databases are useful for characterising welding-induced initial imperfections and for validating numerical computations and empirical formula predictions. However, more test databases are required, as most of the existing ones are based on small-scale structure models and on structures built long time ago. It is therefore necessary to obtain test databases on full-scale structure models made from modern materials. In this study, full-scale structure models were fabricated in a world-class shipyard. The plate thickness was varied while the stiffeners and weld bead length were kept unchanged.

## 2. DESIGN AND FABRICATION OF TEST STRUCTURE

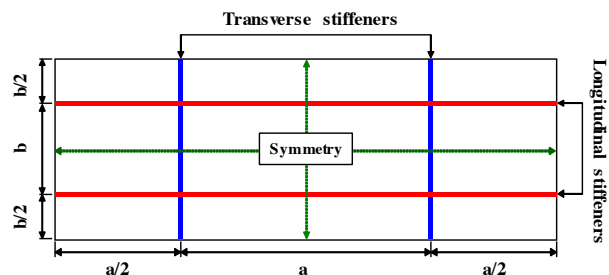
### 2.1 GEOMETRIC PROPERTY

Figure 4 shows the test structure used in this study, which is part of the deck section of a typical LQ of floating, production, storage and offloading units. The structure is composed of plate elements supported by longitudinal and transverse stiffeners.

In real offshore structures, stiffener spacing ranges from 800-1,000 mm, plate length ranges from 1,800-3,600 mm and plate thickness ranges from 6-12 mm.

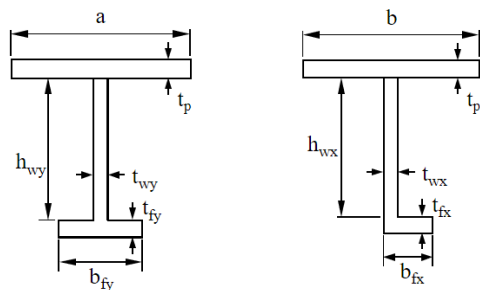


(a) View of stiffened panel



(b) Layout of stiffeners (2-bay model)

Figure 4: Test structure (stiffened panel at deck)



(a) Transverse frame (b) Longitudinal stiffener

Figure 5: Nomenclature of dimension for transverse frame and longitudinal stiffener used in the test structures

Table 1: Dimensions of test structures

Type	$a$ (mm)	$b$ (mm)	$t_p$ (mm)	$L_w$ (mm)	Stiffener Type	$h_w$ (mm)	$t_w$ (mm)	$b_f$ (mm)	$t_f$ (mm)
Deck	3,200	800	6	6.5	Longitudinal (Angle type)	125	7	75	7
			8						
			10		Transverse (T-bar type)	350	12	100	17
			12						

Note:  $L_w$  is the weld bead length (Figure. 6).

Table 1 indicates the overall dimensions of the test structures considered in this study, in which a 1/2+1+1/2-bay model is used in association with longitudinal and transverse stiffeners. The plate length (transverse stiffener spacing) is 3,200 mm and the plate breadth (longitudinal stiffener spacing) is 800 mm. The plate thickness is varied between 6, 8, 10 and 12 mm. Figure 5 shows the types of stiffeners; the angle type is used for longitudinal stiffeners and the T type is used for transverse stiffeners. The dimensions of the longitudinal and transverse stiffeners are fixed, as indicated in Table 1.

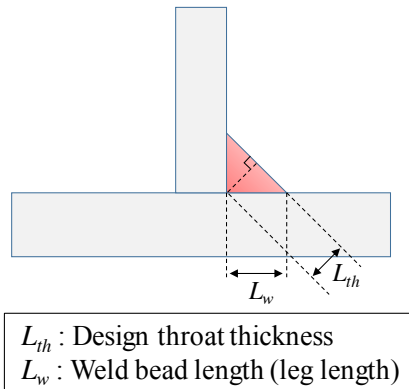


Figure 6: Nomenclature of the weld bead length

## 2.2 MATERIAL PROPERTY

The test structures are made of mild steel with a yield strength of 309 MPa. Table 2 indicates the mechanical properties of the material. In this study, tensile coupon tests were not performed to define the material properties but Table 2 presents nominal values of mechanical properties defined from steel mill certification of steel maker (POSCO steel mill).

## 2.3 TEST STRUCTURE FABRICATION

The test structures are fabricated using exactly the same method used in real shipyards. Stiffeners are attached by continuous fillet welding where the watertight requirements are satisfied (NORSOK, 2011).

The FCAW method is widely adopted in the construction of offshore structures due to its productivity and convenience. Auto-carriage welding is the most widely used technique for attaching stiffeners to plating, as shown in Figure 7. To construct LQ structures, tack welding is first performed to attach the plating and stiffeners at an appropriate pitch (distance) at the tack welding points. Auto-carriage welding is then performed to attach the stiffeners to the plating, with the intended weld bead length maintained along the stiffeners, as specified in the WPS requirements. The remaining sections at the end of the welding area or where the stiffeners overlap are welded manually in accordance

with the WPS requirements. Figure 8 shows the individual steps of the welding procedure used in the fabrication of the test structures.

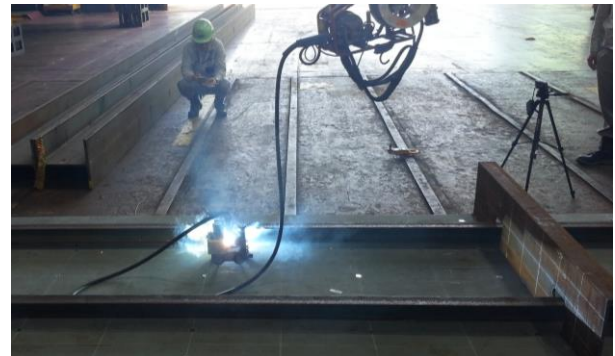
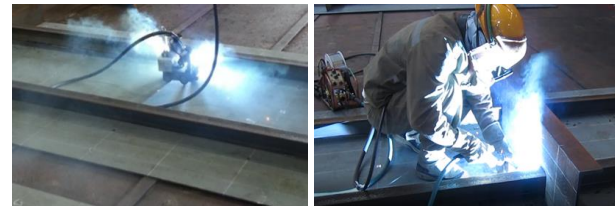


Figure 7: Use of auto-carriage welding



(a) Setting of stiffener

(b) Tack welding



(c) Auto-carriage welding

(d) Manual welding

Figure 8: Welding steps for fabricating the test structures

## 2.4 WELD BEAD LENGTH

The weld bead length (leg length), illustrated in Figures 6 and 9, is an important parameter used in the welding process. It varies with heat input, among other factors. Table 3 summarises the welding parameters used in the fabrication of the test structures where the weld bead length was fixed at 6.5 mm with a single pass welding regardless of different plate thicknesses.

The weld bead length is in fact determined to meet the minimum requirements of class rules. In reality, however, a larger weld bead length than the minimum class rule requirement is usually applied because ship owners ask for applying larger weld bead length to assure better weldability and defect free weld. In shipbuilding industry practice, a weld bead length of 6 – 6.5 mm is usually applied for 6 – 12 mm thick plate panels as far as a single pass welding is considered. In this regard, the weld bead length of 6.5 mm applied to fabricate the test structures is considered to be reasonably practicable.

Table 2: Overall characteristics of mechanical properties

Kind of material	$E$ (GPa)	$\sigma_y$ (MPa)	$\sigma_u$ (MPa)	$\nu$ (-)	$\epsilon_f$ (mm/mm)
Mild A	203	309	458	0.3	0.23

Note:  $E$  is the elastic modulus,  $\sigma_y$  is the yield strength,  $\sigma_u$  is the ultimate tensile strength,  $\nu$  is the Poisson ratio and  $\epsilon_f$  is the fracture strain (elongation).

Table 3: Welding parameters for weld bead length

$L_w$ (mm)	Current (A)	Voltage (V)	Speed (CPM)	Speed (mm/s)	Heat input (KJ/mm)
6.5	320	32	36	6.0	1.71

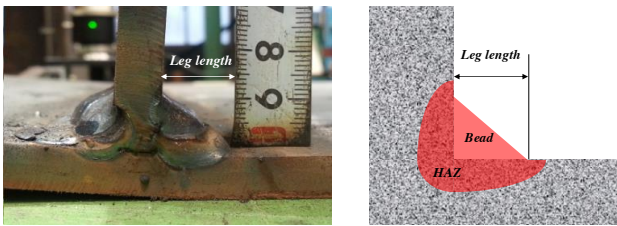
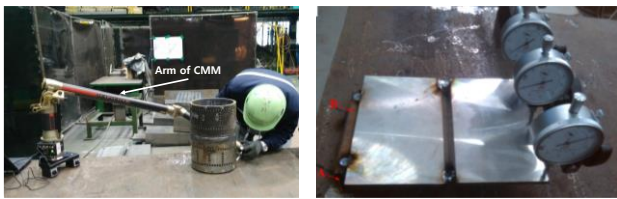


Figure 9: Real view and schematic definition of weld bead length



(a) CMM measuring method

(b) Dial gauge measuring method (Wang et al. 2015)

Figure 10: Contact methods for measuring initial deflections

### 3. MEASUREMENT OF WELDING-INDUCED INITIAL DEFLECTIONS

#### 3.1 MEASURING METHOD

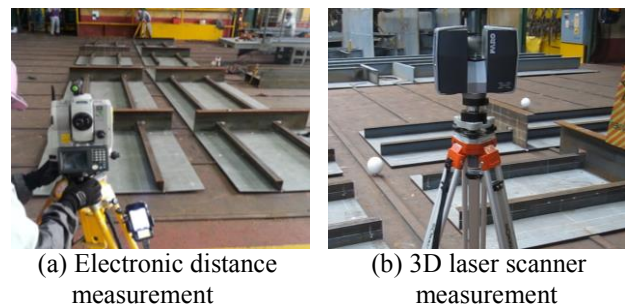
There are many methods to measure the deflection caused by welding. There are two classes of measurement methods: contact methods that directly touch the structure during the measurement and non-contact methods that do not physically contact the structure.

There are two common contact measurement methods; one uses Coordinate Measuring Machine (CMM) equipment and the other uses dial gauges (Figure 10). CMM equipment can very precisely measure the deformation of a structure (tolerance about 0.01mm).

However, as shown in Figure 10(a), the measurement range is limited by the arm length of the CMM equipment. The dial gauge method is the classic method for measuring welded plate. The equipment is convenient

to install and it has the advantage of checking the real time deformation of the measurement structures. However, it is not used frequently, because it is associated with many human errors in equipment installation and measurement.

There are two common non-contact measurement methods: electronic distance measurement and 3-dimensional (3D) laser scanning (Figure 11). Although it is inconvenient to attach the target to the position of the object being measured when using the electronic distance measurement method, it is the common method for field measurements (e.g., in civil engineering, shipbuilding, construction, air-craft, plants etc.)



(a) Electronic distance measurement

(b) 3D laser scanner measurement

Figure 11: Non-contact methods for measuring initial deflections

In addition, the measurement accuracy of this instrument is excellent (accuracy range is about 0.8 to 1 mm). The 3D laser scanning method is a relatively new method. It acquires the 3D shape of the object being measured by using the laser to secure the 3D point data. However, the time required for measuring and post-processing is relatively long. Also, the accuracy range of is about 5 mm, which is larger than that of the electronic distance measurement method. For this reason, this study uses electronic distance measurement to measure the initial deflection caused by stiffened welding.

Three-dimensional configurations of the test structures are measured before and after welding using an electronic theodolite (transit) technique integrated with an electronic distance measurement, where the slope distances are detected from the instrument to a particular point. An on-board computer collects the measurement data and

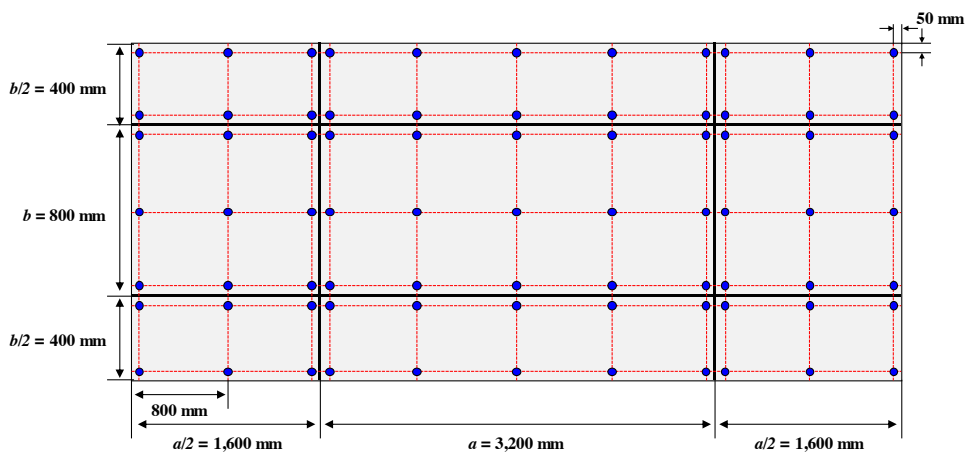
performs advanced coordinate-based calculations. This technique is useful for measuring the 3D coordinates of target objects (Kavanagh and Glenn, 1996).

Table 4 provides an example of the measuring equipment used in this study. As shown in Figure 12, 77 points are targeted for measurement. Figure 13 shows the process

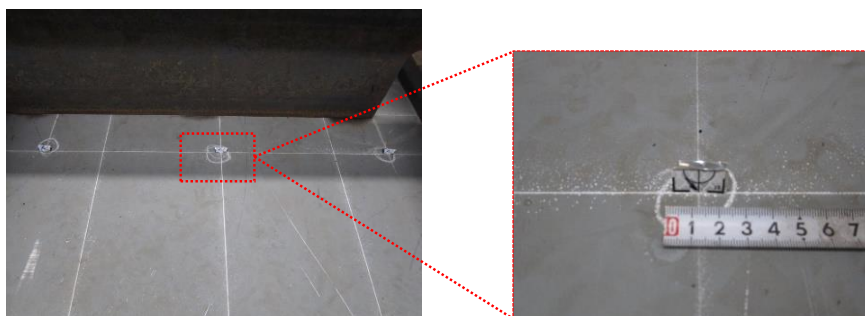
used to measure the welding-induced initial deflections. For the ultimate strength analysis of plate elements, the relative values of initial deflections with respect to support members at (four) plate boundaries are important (Paik, 2018). In this regard, the relative values of plate initial deflections were measured so that the initial deflections at the plate boundaries are zero.

Table 4: Specifications of the equipment used for measuring the initial deflections

	Measuring equipment : NET05X (©SOKKIA)	
	Magnification	× 30
	Resolving power	2.5 inch
	Minimum focus	4.3 ft
	Angle measurement accuracy	0.5 inch
	Distance measurement range	4.3 to 650 ft



(a) Location of 77 measuring points



(b) Details of a sample measuring point

Figure 12: Reference points defined for measuring the initial deflections

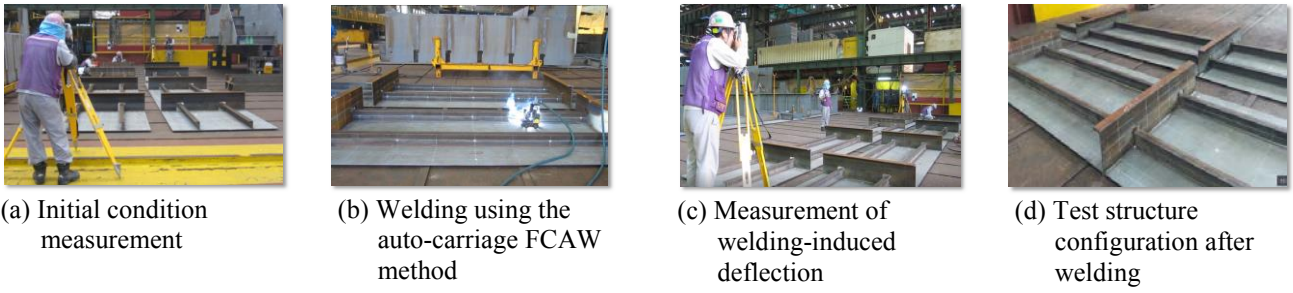


Figure 13: Procedure for measuring the initial deflections

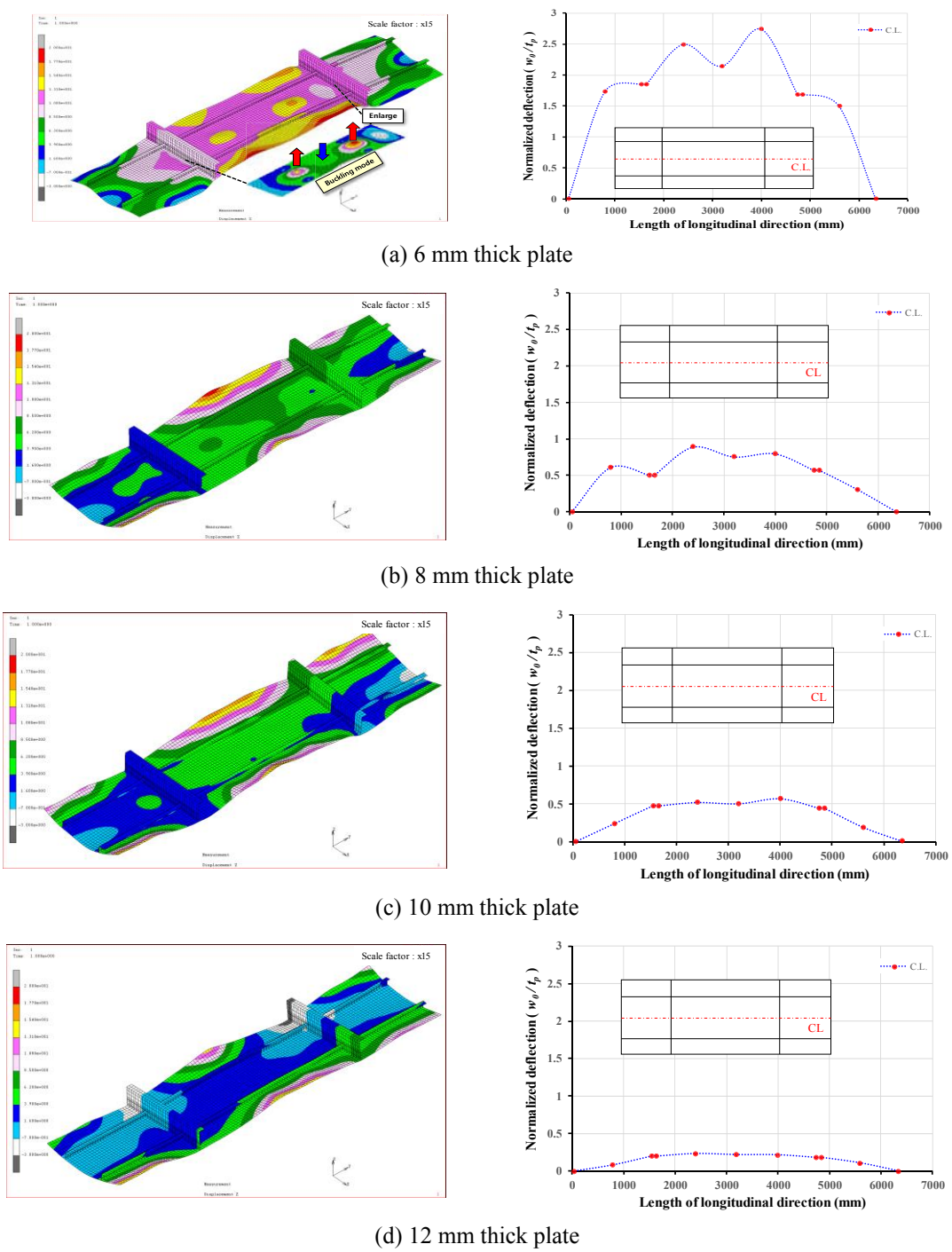
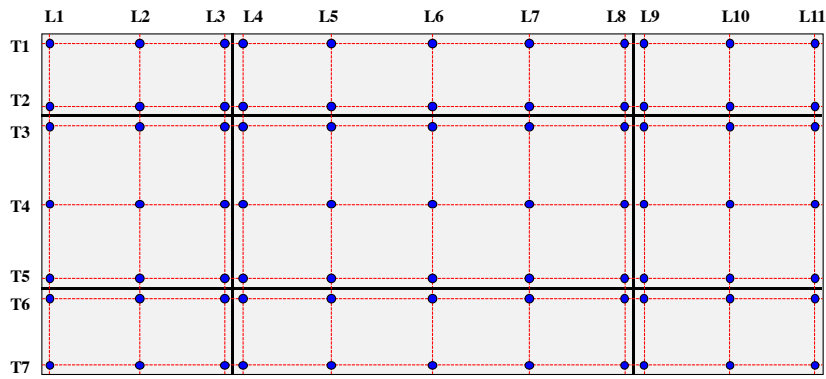


Figure 14: Pattern and magnitude of measured initial deflections normalized by the plate thickness

Table 5: Measured database of the plate initial deflections normalized by the plate thickness



(a) Plate initial deflection for 6 mm thick plate

Plate initial deflections ( $w_0/t_p$ )			Longitudinal direction ( $x = 0 \sim 6,400$ mm)										
			50	800	1,550	1,650	2,400	3,200	4,000	4,750	4,850	5,600	6,350
			L1	L2	L3	L4	L5	L6	L7	L8	L9	L10	L11
Transverse direction ( $y = 0 \sim 1,600$ mm)	50	T1	0.32	0.29	1.77	1.82	2.42	2.01	2.52	2.07	1.82	1.26	0.66
	350	T2	1.12	1.43	1.75	1.81	2.04	2.03	2.07	1.93	1.87	1.65	1.37
	450	T3	1.13	1.53	1.79	1.80	1.89	2.03	1.90	1.88	1.92	1.69	1.35
	800	T4	0.00	1.74	1.86	1.86	2.50	2.14	2.74	1.69	1.69	1.50	0.00
	1,150	T5	0.64	1.22	1.78	1.76	1.94	2.20	1.98	1.87	1.84	1.39	0.84
	1,250	T6	0.87	1.33	1.67	1.75	2.23	2.26	2.29	1.93	1.81	1.42	0.99
	1,550	T7	1.17	0.09	1.45	1.81	3.09	2.55	3.19	2.08	1.66	0.48	0.95

(b) Plate initial deflection for 8 mm thick plate

Plate initial deflections ( $w_0/t_p$ )			Longitudinal direction ( $x = 0 \sim 6,400$ mm)										
			50	800	1,550	1,650	2,400	3,200	4,000	4,750	4,850	5,600	6,350
			L1	L2	L3	L4	L5	L6	L7	L8	L9	L10	L11
Transverse direction ( $y = 0 \sim 1,600$ mm)	50	T1	1.02	1.14	0.49	0.46	1.14	2.23	1.83	1.02	0.98	1.36	0.95
	350	T2	0.42	0.42	0.45	0.47	0.77	0.99	1.10	0.92	0.88	0.76	0.63
	450	T3	0.38	0.42	0.47	0.48	0.65	0.92	0.92	0.84	0.87	0.76	0.59
	800	T4	0.00	0.61	0.50	0.50	0.89	0.75	0.80	0.57	0.57	0.30	0.00
	1,150	T5	0.33	0.41	0.45	0.47	0.61	0.70	0.78	0.72	0.72	0.49	0.24
	1,250	T6	0.59	0.56	0.44	0.48	0.61	0.87	0.90	0.71	0.67	0.61	0.45
	1,550	T7	1.88	1.71	0.53	0.47	0.67	1.78	1.34	0.68	0.61	1.24	1.27

(c) Plate initial deflection for 10 mm thick plate

Plate initial deflections ( $w_0/t_p$ )			Longitudinal direction ( $x = 0 \sim 6,400$ mm)										
			50	800	1,550	1,650	2,400	3,200	4,000	4,750	4,850	5,600	6,350
			L1	L2	L3	L4	L5	L6	L7	L8	L9	L10	L11
Transverse direction ( $y = 0 \sim 1,600$ mm)	50	T1	1.05	1.02	0.40	0.37	0.95	1.56	1.55	0.86	0.82	1.55	1.33
	350	T2	0.41	0.36	0.34	0.35	0.60	0.71	0.84	0.68	0.68	0.70	0.73
	450	T3	0.33	0.31	0.33	0.37	0.50	0.57	0.59	0.63	0.63	0.63	0.64
	800	T4	0.00	0.24	0.47	0.47	0.52	0.50	0.57	0.44	0.44	0.19	0.00
	1,150	T5	0.29	0.28	0.30	0.29	0.42	0.48	0.42	0.28	0.29	0.14	-0.04
	1,250	T6	0.51	0.43	0.30	0.30	0.55	0.59	0.56	0.28	0.24	0.19	0.11
	1,550	T7	1.49	1.25	0.28	0.25	0.99	1.58	1.11	0.23	0.08	0.69	0.71

(d) Plate initial deflection for 12 mm thick plate (Table 5 continued)

Plate initial deflections ( $w_0/t_p$ )			Longitudinal direction ( $x = 0 \sim 6,400$ mm)										
			50	800	1,550	1,650	2,400	3,200	4,000	4,750	4,850	5,600	6,350
			L1	L2	L3	L4	L5	L6	L7	L8	L9	L10	L11
Transverse direction ( $y = 0 \sim 1,600$ mm)	50	T1	0.41	0.31	-0.13	-0.14	0.37	1.04	0.25	-0.29	-0.24	0.41	0.72
	350	T2	0.10	0.00	-0.06	-0.05	0.19	0.33	0.13	-0.08	-0.11	0.00	0.18
	450	T3	0.07	0.02	-0.02	-0.03	0.15	0.27	0.09	-0.03	-0.06	-0.02	0.12
	800	T4	0.00	0.08	0.20	0.20	0.23	0.22	0.22	0.18	0.18	0.11	0.00
	1,150	T5	0.39	0.28	0.20	0.20	0.21	0.39	0.35	0.37	0.38	0.32	0.27
	1,250	T6	0.55	0.41	0.24	0.23	0.29	0.55	0.55	0.45	0.42	0.44	0.40
	1,550	T7	1.21	1.13	0.34	0.33	0.49	1.19	1.07	0.65	0.61	0.92	0.82

3.2 MEASUREMENT RESULTS OF WELDING-INDUCED DEFLECTIONS

Figure 14 shows the measurement results for the test structures' welding-induced deflections (normalized results). For a given leg length, It is considered that the plate thickness and deformation are interrelated.

Specifically, the out-of-plane deformation (plate initial deflection) caused by welding increases as the thickness of the plate decreases. A buckling mode is observed on the inside of the stiffener of the 6 mm thick plate rather than the usual welding deflection. The measured database of the initial deflection is provided in Table 5.

4. MEASUREMENT OF WELDING INDUCED RESIDUAL STRESSES

4.1 METHOD OF MEASUREMENT

There are various methods for measuring the residual stress of the plate caused by welding. Although there are different classification methods based on various criteria, this study divides them into destructive and non-destructive methods. A typical destructive method for measuring the residual stress is the hole drilling method that uses strain gages. To measure the residual stress, a strain gauge is attached to the surface of the structure and holes are drilled to a certain depth. The residual stress is calculated by measuring the strain generated at the gauges.

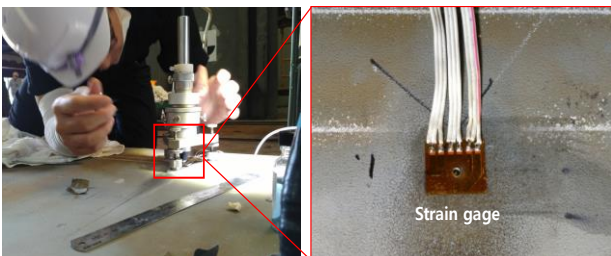


Figure 15: Destructive method for measuring residual stress (hole drilling)

It is the traditional method and the only one recognised as reliable by the ASTM E-837 standard. However, many human errors occur during the process of attaching and

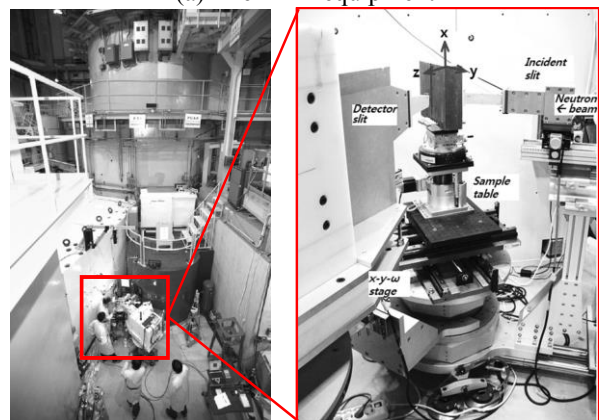
drilling the strain gages. The details of this method are shown in Figure 15.

Common non-destructive methods for measuring residual stress include XRD and neutron diffraction. The details of these instruments are shown in Figure 16.

In the XRD method, the metal microstructure of the surface and the surface of the structure are irradiated with X-rays, and then X-ray diffraction is calculated according to the Bragg's rule to measure the distance between the lattice planes. It is widely used for measuring structures and surface residual stresses, as it is simple and highly reliable.



(a) The XRD equipment



(b) Neutron diffraction: Research reactor HANARO in Korea Atomic Energy Research Institute (Woo et al. 2015)

Figure 16: Non-destructive method for measuring residual stress (XRD and neutron diffraction)

The neutron diffraction method is a recently developed measurement method. The measurement principle is the same as in the XRD method, but the particle used in the irradiation is a neutron. The advantage of this method is that, unlike XRD, it can reliably measure the residual stresses in relatively thick structures (over 10 mm of thickness). However, it has disadvantages such as the high price and large size of the neutron irradiation equipment, and it can only be used to measure specimen units in laboratory settings.

Therefore, this study uses the XRD method to measure the residual stress of the plate caused by the stiffener welding. The measurement principle of XRD is based on the known characteristics of XRD. Bragg's law is expressed as follows:

$$2d \sin \theta = n\lambda \quad (1)$$

where  $d$  is the lattice space,  $\theta$  is the incident angle and the reflection angle,  $\lambda$  is the wavelength of the X-ray and  $n$  is an integer denoting the order of diffraction. A description of this rule is provided in Figure 17.

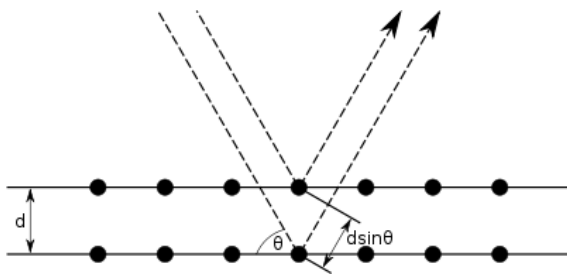


Figure 17: Law of XRD (Bragg's law)

If a metal object that is polycrystallised by welding is deformed so that it has a uniform strain, the material will have a certain residual stress. This new residual stress changes the lattice spacing.

This new lattice spacing is almost constant in all of the crystal grains on the surfaces with similar directions, and the diffracted ray that is irradiated at this time shifts to show a new  $\theta$  position. If the metal is plastic deformed, the lattice spacings of the faces exhibit different values depending on the orientation of the grain. This altered lattice spacing moves the diffraction line.

In other words, the XRD system estimates the residual stress by measuring the lattice spacing of individual crystal grains, as each crystal grain changes according to the stress-induced orientation. The specifications of the XRD method are given in Table 6.

Figure 18 shows the longitudinal and transverse points for measuring residual stress caused by welding. The residual stress measurements are performed at 15 points (8 points in the longitudinal direction and 7 points in the transverse direction) for each thickness. In the XRD residual stress measurement system, the penetration of the X-rays is approximately  $5 \mu\text{m}$  below the surface. That is, the residual stress measurement is performed on the crystal grains in a cylindrical volume with a diameter of 3 mm and a depth of  $5 \mu\text{m}$  (Xstress, 2010).

When the metallic material is plastic deformed, the residual stresses at the surface and those directly below the surface are different. The XRD measures the residual stress at the surface. As the reliability of the residual stress depends on the surface roughness condition, the influence of surface roughness should be minimised by maintaining a surface shape with a constant roughness. Accordingly, electrolytic polishing is carried out at the residual stress measurement positions to remove any fine mechanical damage on the surface and maintain an even condition on the surface of the measured object.

Figure 19 shows the calibration, the first step in the XRD measurement method. Figure 20 shows the measurement of the residual stresses in three directions, i.e., 0, 45 and 90 degrees, at each measurement point.

Table 6: Specification of the XRD equipment

		Residual stress measuring equipment: Xstress3000 (©Stresstech)	
		Goniometer	
Inclination		-45 ~ +45 degree	
Oscillation		0 ~ 6 degree	
Accuracy		-0.003 ~ +0.003 mm	
		Detector	
Angular resolution		0.029 degree/pixel mm	
Range		100~165 degree	

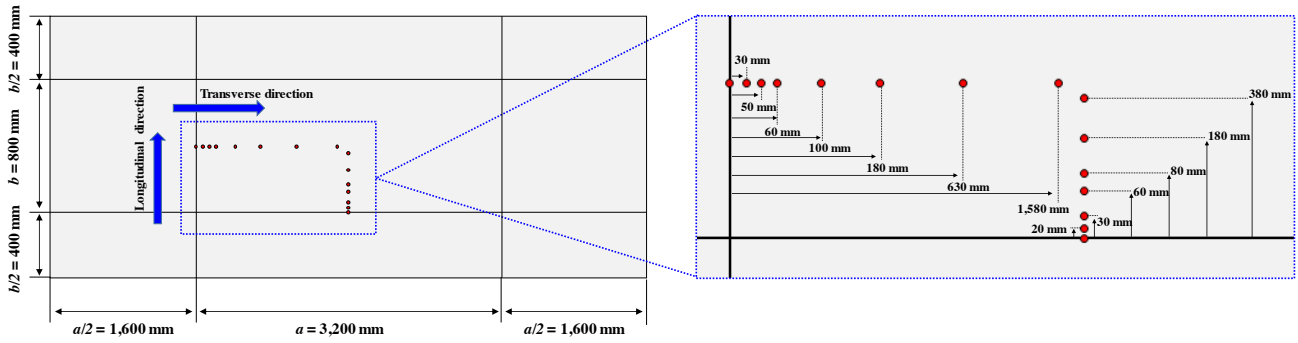


Figure 18: Reference points of measuring residual stresses using the XRD method

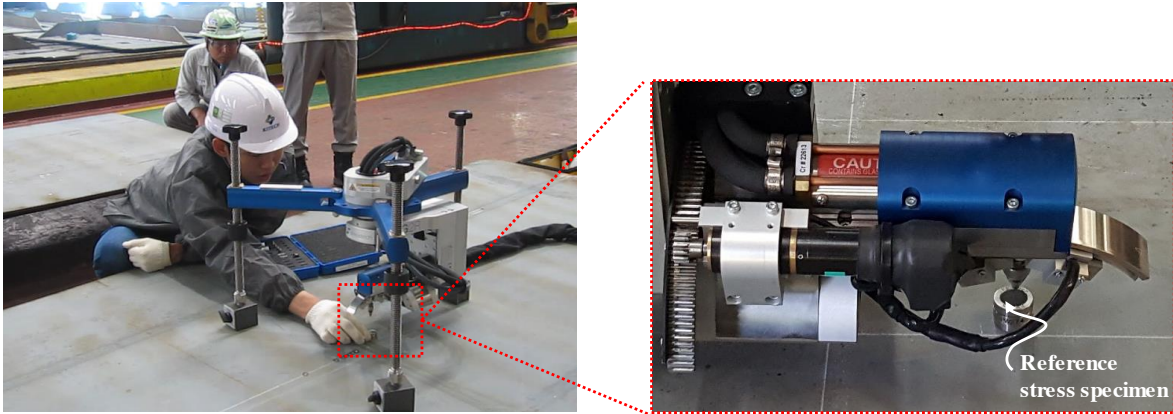
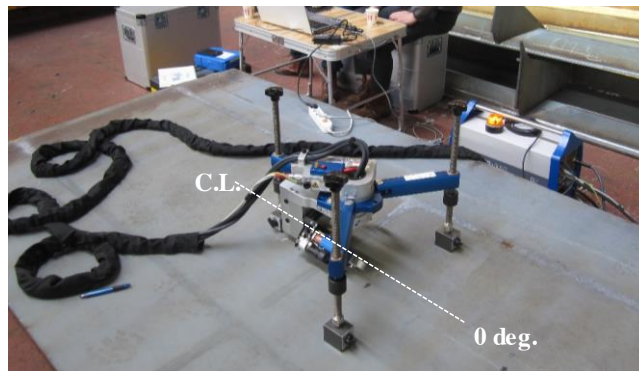


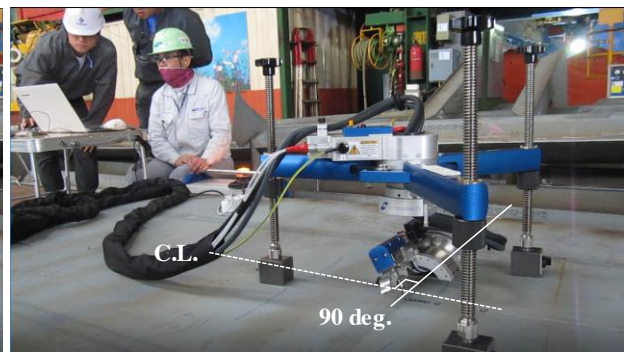
Figure 19: Calibration using a reference specimen



(a) Measurement at an angle of 0 deg.



(b) Measurement at an angle of 45 deg.



(c) Measurement at an angle of 90 deg.

Figure 20: Residual stress measurement at three angles

#### 4.2 RESULTS OF RESIDUAL STRESS MEASUREMENTS

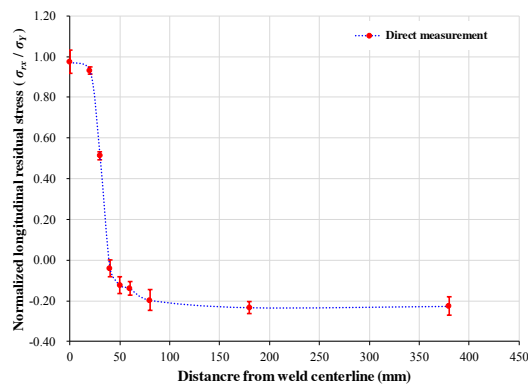
The measured database of the residual stresses is provided in Table 8. Figure 21 plots the distributions of the residual stresses for different plate thicknesses. It is found that the tensile residual stresses develop in heat-affected zones and the compressive residual stresses exist to achieve a self-equilibrium condition in the plane of the plate. Also, it is observed that the magnitude of the tensile residual stress blocks reaches the yield strength of material. The axial compressive stress values developed in the middle of the plate decrease as the plate thickness increases. It is obvious that the residual stresses develop not only in the longitudinal direction but also in the transverse directions as both longitudinal stiffeners and transverse frames have been attached by welding. In this regard, thin plates can buckle under biaxial compressive residual stresses during the welding process. The authors have performed benchmark studies in a separate paper (Yi et al., 2018) where thermo-elastic-plastic finite element method computations were compared with the present test data, showing that both are in very good agreement.

Figure 22 presents the relations between the breadth of the heat-affected zones in the longitudinal or transverse direction versus the plate thickness where the breadth of

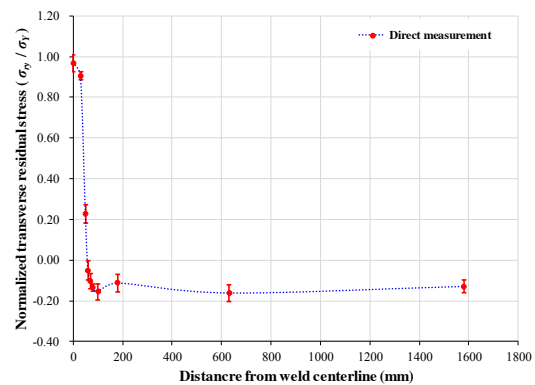
the heat-affected zone is defined by the breadth that the tensile residual stress block is developed. The heat-affected zone is formed with a band width, in which the stress is approximately equal to the tensile yield stress because the molten metal can expand freely, as a liquid, whereas after welding it quickly reverts to a solid and the shrinkage that occurs during cooling involves “plastic flow”. It is seen that the breadth of the heat-affected zone is not affected by the plate thickness but it is affected by the plate slenderness ratio involving the plate length (or breadth) and the material yield strength as well as the weld bead length, among other factors. Similar observations are found in welded aluminium plate structures (Paik, 2008). It is realized that the breadth of the heat-affected zone for the test structures is 30 mm in the plate breadth direction and 50 mm in the plate length direction.

With the nomenclature presented in Figure 23, the breadths of the heat-affected zone can be given from the equilibrium condition between the tensile residual stress block and the compressive residual stress block as follows (Paik 2018):

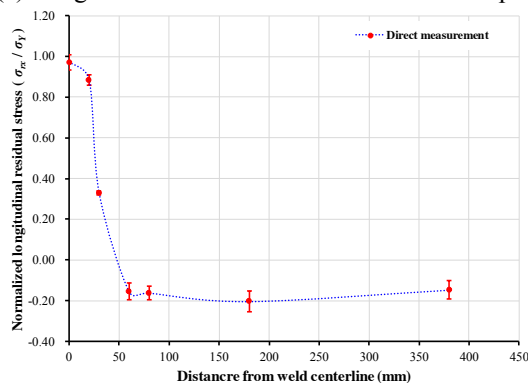
$$2b_t = \frac{\sigma_{rcx}}{\sigma_{rcx} - \sigma_{rtx}} b, \quad 2a_t = \frac{\sigma_{rcy}}{\sigma_{rcy} - \sigma_{rty}} a \quad (2)$$



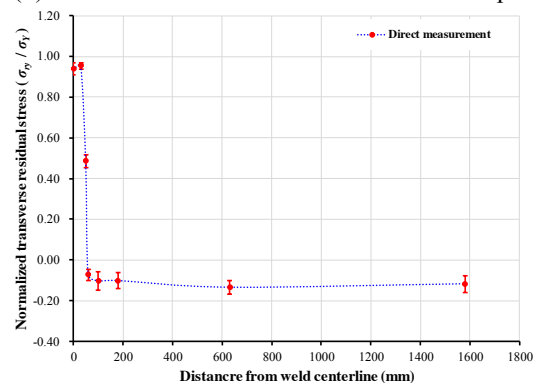
(a) Longitudinal residual stress for 6 mm thick plate



(b) Transverse residual stress for 6 mm thick plate

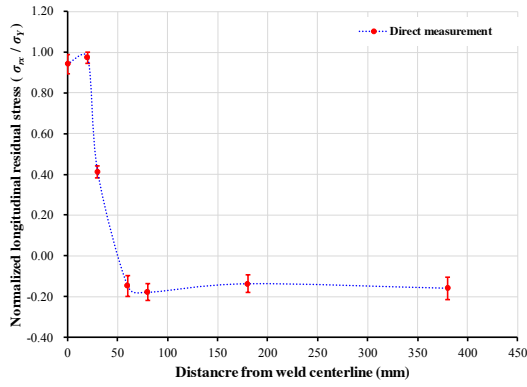


(c) Longitudinal residual stress for 8 mm thick plate

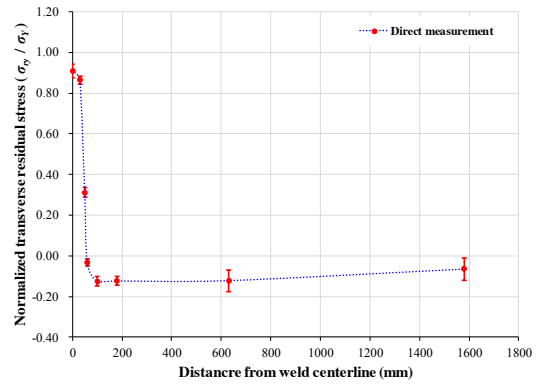


(d) Transverse residual stress for 8 mm thick plate

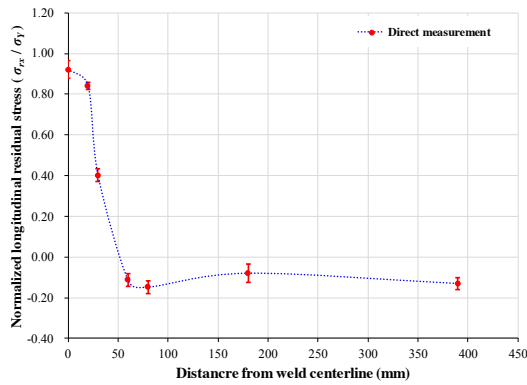
Figure 21: Pattern and magnitude of residual stress measurements normalized by the yield stress (parts a-d of a-h)



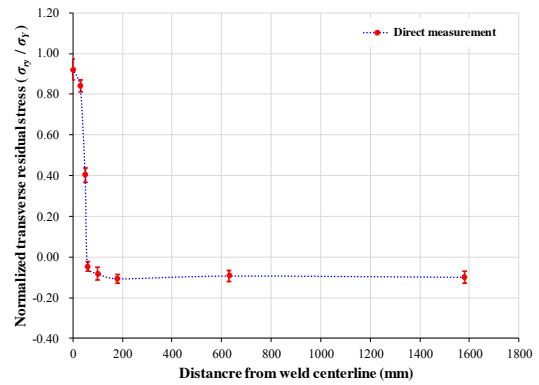
(e) Longitudinal residual stress for 10 mm thick plate



(f) Transverse residual stress for 10 mm thick plate



(g) Longitudinal residual stress for 12 mm thick plate



(h) Transverse residual stress for 12 mm thick plate

Figure 21: Pattern and magnitude of residual stress measurements normalized by the yield stress

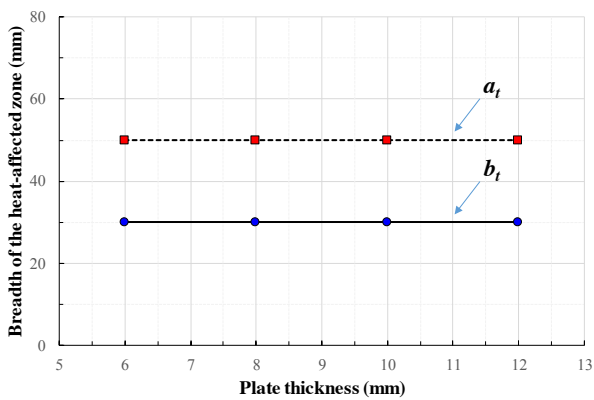


Figure 22: The relation between the breadth of the heat-affected zone versus the plate thickness

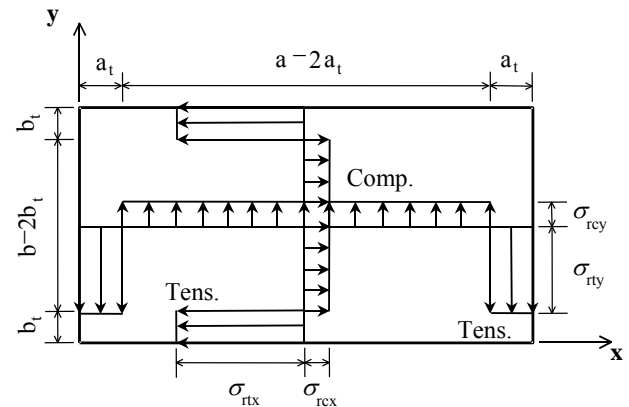


Figure 23: Schematic distribution of welding-induced residual stresses in stiffened plate structures (Paik, 2018)

Table 8: Measured database of the residual stresses

(a) Longitudinal residual stress for 6 mm thick plate

Distance from weld center line (mm)	Longitudinal residual stress $\sigma_{rx}$ (MPa)	$\sigma_{rx} / \sigma_Y$
0	301.0	0.97
20	288.0	0.93
30	158.4	0.51
40	-12.5	-0.04
50	-38.1	-0.12
60	-42.8	-0.14
80	-60.7	-0.20
180	-72.0	-0.23
380	-70.0	-0.22

(b) Transverse residual stress for 6 mm thick plate

Distance from weld center line (mm)	Transverse residual stress $\sigma_{ry}$ (MPa)	$\sigma_{ry} / \sigma_Y$
0	299.0	0.97
30	280.0	0.91
50	69.8	0.23
60	-15.6	-0.05
70	-32.0	-0.10
80	-42.1	-0.14
100	-48.0	-0.16
180	-35.2	-0.11
630	-50.0	-0.16
1,580	-40.2	-0.13

(c) Longitudinal residual stress for 8 mm thick plate

Distance from weld center line (mm)	Longitudinal residual stress $\sigma_{rx}$ (MPa)	$\sigma_{rx} / \sigma_Y$
0	300.2	0.97
20	273.4	0.88
30	102.1	0.33
60	-48.0	-0.16
80	-50.2	-0.16
180	-63.1	-0.20
380	-45.7	-0.15

(d) Transverse residual stress for 8 mm thick plate

Distance from weld center line (mm)	Transverse residual stress $\sigma_{ry}$ (MPa)	$\sigma_{ry} / \sigma_Y$
0	290.2	0.94
30	295.1	0.95
50	150.0	0.49
60	-22.5	-0.07
100	-32.2	-0.10
180	-31.8	-0.10
630	-42.2	-0.14
1,580	-36.7	-0.12

(e) Longitudinal residual stress for 10 mm thick plate

Distance from weld center line (mm)	Longitudinal residual stress $\sigma_{rx}$ (MPa)	$\sigma_{rx} / \sigma_Y$
0	291.0	0.94
20	301.2	0.97
30	127.8	0.41
60	-45.8	-0.15
80	-55.4	-0.18
180	-42.5	-0.14
380	-49.3	-0.16

(f) Transverse residual stress for 10 mm thick plate

Distance from weld center line (mm)	Transverse residual stress $\sigma_{ry}$ (MPa)	$\sigma_{ry} / \sigma_Y$
0	281.1	0.91
30	267.2	0.86
50	96.1	0.31
60	-10.2	-0.03
100	-38.7	-0.13
180	-38.0	-0.12
630	-37.5	-0.12
1,580	-20.2	-0.06

(g) Longitudinal residual stress for 12 mm thick plate

Distance from weld center line (mm)	Longitudinal residual stress $\sigma_{rx}$ (MPa)	$\sigma_{rx} / \sigma_Y$
0	284.7	0.92
20	260.3	0.84
30	124.3	0.40
60	-34.8	-0.11
80	-45.7	-0.15
180	-24.6	-0.08
380	-40.2	-0.13

(h) Transverse residual stress for 12 mm thick plate

Distance from weld center line (mm)	Transverse residual stress $\sigma_{ry}$ (MPa)	$\sigma_{ry} / \sigma_Y$
0	284.6	0.92
30	260.1	0.84
50	124.7	0.40
60	-14.5	-0.05
100	-25.5	-0.08
180	-33.1	-0.11
630	-28.9	-0.09
1,580	-30.8	-0.10

## 5. CONCLUSIONS

The objectives of the present study have been to obtain the full scale measurement database of the weld-induced initial imperfections (initial deflections and residual stresses) in steel stiffened plate structures. For the purpose of parametric studies, the plate thickness was varied at 6mm, 8mm, 10mm and 12mm, while the types of longitudinal stiffeners (with angle type) and transverse frames (with T type) were identical and also the weld bead length was applied with 6.5mm. Based on the study, the following conclusions can be drawn.

(1) The methods for measuring the residual stresses and the initial deflections caused by welding were presented. In the present measurements, the non-contact method was used for measuring the plate initial deflections and the XRD method was used for measuring the residual stresses. It is found that the measuring methods applied in the present study are useful to figure out the complexity in the pattern and magnitude of the weld-induced initial imperfections and also in geometry of stiffened plate structures.

(2) The measured database of the plate initial deflections with varying plate thickness was tabulated in the paper. As well recognized in industry practices, it is found that the magnitude of the plate initial deflections increases as the plate thickness decreases. Also, the pattern of the plate initial deflections is more complex in thin plates than in thick plates. It is realized that the plate buckling mode of the plate initial deflections becomes dominant as the plate thickness decreases. This may imply that thin plates have buckled during the welding process. This is due to the fact that the biaxial compressive residual stresses can reach the elastic buckling strength criteria for thin plates.

(3) The measured residual stresses with varying the plate thickness was tabulated in the paper. As again well recognized in industry practices, it is found that the tensile residual stresses develop in the heat-affected zones and the compressive residual stresses exist to achieve a self-equilibrium condition in the plane of the plate. It is observed that the magnitude of the tensile residual stress blocks reaches the yield strength of material. It tends that the compressive residual stresses increases as the plate thickness decreases. Also, it is obvious that the residual stresses develop not only in the longitudinal direction but also in the transverse directions as both longitudinal stiffeners and transverse frames have been attached by welding. As mentioned in (2) above, thin plates can buckle under biaxial compressive residual stresses during the welding process.

(4) The full scale measurement database of weld-induced initial imperfections is very demanding for the buckling and ultimate strength computations and design of steel stiffened plate structures such as ships and offshore structures. The main contributions of the present paper

are to obtain such database which should be very useful for practicing engineers and academia in terms of not only robust structural analysis and design but also weld-induced initial imperfection predictions.

## 6. ACKNOWLEDGEMENTS

The authors are grateful to Samsung Heavy Industries for supporting the research. The present study was undertaken at the International Centre for Advanced Safety Studies which has been a Lloyd's Register Foundation Research Centre of Excellence.

## 7. REFERENCES

1. BRUNO, G., YORDAN, G. & SOARES, C.G. (2011). Effect of weld shape imperfections on the structural hot-spot stress distribution, *Ships and Offshore Structures*, 6(1-2): 145-159.
2. CHEN, B.Q., HASHEMZADEH, M. & GUEDES, SOARES C. (2018) Validation of numerical simulations with X-ray diffraction measurements of residual stress in butt-welded steel plates, *Ships and Offshore Structures*, 13(3): 273-282.
3. CHENG, J.J.R., ELWI, A.E., GRODIN, G.Y. & KULAK, G.L. (1996). Material testing and residual stress measurements in a stiffened steel plate. In: *Strength and Stability of Stiffened Plate Components*. Ship Structure Committee, SSC-399, Washington, DC.
4. EGGERT, L., FRICKE, W. & PAETZOLD, H. (2012). Fatigue strength of thin-plated block joints with typical shipbuilding imperfections. *Welding in the World*, 56(11-12): 119-128.
5. FARAJKHAH, V., LIU, Y. & GANNON, L. (2016). Finite element study of 3D simulated welding effect in aluminium plates, *Ships and Offshore Structures*, 12(2): 196-208.
6. GANNON, L.G., LIU, Y., PEGG, N.G. & SMITH, M.J. (2012a). Effect of three-dimensional welding-induced residual stress and distortion fields on strength and behaviour of flat-bar stiffened panels, *Ships and Offshore Structures*, 8(5): 565-578.
7. GANNON, L.G., PEGG, N.G., SMITH, M.J. & LIU, Y. (2012b). Effect of residual stress shakedown on stiffened plate strength and behaviour, *Ships and Offshore Structures*, 8(6): 638-652.
8. GANNON, L., LIU, Y., PEGG, N. & SMITH, M.J. (2015). Nonlinear collapse analysis of stiffened plates considering welding-induced residual stress and distortion, *Ships and Offshore Structures*, 11(3): 228-244.
9. KAVANAGH, B.F. & GLENN BIRD, S.J. (1996). *Surveying Principles and Applications* (4 Ed.). Prentice Hall, pp. 257-264.

10. KHAN, I. & ZHANG, S. (2011). Effects of welding-induced residual stress on ultimate strength of plates and stiffened panels, *Ships and Offshore Structures*, 6(4): 297-309.
11. KENNO, S.Y., DAS, S., KENNEDY J, ROGGE, R. & GHARGHOURI, M. (2010). Distributions of residual stresses in stiffened plates with one and two stiffeners, *Ships and Offshore Structures*, 5(3): 211–225.
12. KENNO, S.Y., DAS, S., ROGGE, R.B. & GHARGHOURI, M. (2017). Changes in residual stresses caused by an interruption in the weld process of ships and offshore structures, *Ships and Offshore Structures*, 12(3): 341–359.
13. KHEDMATI, M.R., PEDRAM, M. & RIGO, P. (2012). The effects of geometrical imperfections on the ultimate strength of aluminium stiffened plates subject to combined uniaxial compression and lateral pressure, *Ships and Offshore Structures*, 9(1): 88-109.
14. LILLEMÄE, I., LIINALAMPI, S., REMES, H., ITÄVUO, A. & NIEMELÄ, A. (2017). Fatigue strength of thin laser-hybrid welded full-scale deck structure, *International Journal of Fatigue*, 95: 282-292.
15. LUÍS, R.M., SOARES, C.G. & NIKOLOV, P.I. (2009). Collapse strength of longitudinal plate assemblies with dimple imperfections, *Ships and Offshore Structures*, 3(4): 359-370.
16. MASUBUCHI, K. (1980). *Analysis of Welded Structures: Residual Stresses, Distortion and Their Consequences*. Pergamon Press, England & Oxford, U.K.
17. MATSUI, S. (1983). Control of weld distortion in thin-skin welded structures, *Journal of Welding and Joining*, 53(5): 58-66.
18. NORSOK (2011). NORSOK Standard M-101: Structural Steel Fabrication. NORSOK, Oslo, Norway.
19. PAIK, J.K. (2007a). Practical techniques for finite element modeling to simulate structural crashworthiness in ship collisions and grounding (Part I: Theory), *Ships and Offshore Structures*, 2(1): 69-80.
20. PAIK, J.K. (2007b). Practical techniques for finite element modeling to simulate structural crashworthiness in ship collisions and grounding (Part II: Verification), *Ships and Offshore Structures*, 2(1): 81-85.
21. PAIK, J.K. (2007c). Characteristics of welding induced initial deflections in welded aluminium plates, *Thin-Walled Structures*, 45: 493-501.
22. PAIK, J.K. (2008). Mechanical collapse testing on aluminium stiffened panels for marine applications. Ship Structure Committee, SSC-451, Washington, DC.
23. PAIK, J.K. (2018). *Ultimate limit state analysis and design of plated structures*, 2<sup>nd</sup> Edition, John Wiley & Sons, Chichester, UK.
24. PAIK, J.K., ANDRIEU, C. & COJEEN, H.P. (2008). Mechanical collapse testing on aluminium stiffened plate structures for marine applications, *Marine Technology*, 45(4): 228-240.
25. PAIK, J.K. & FRIEZE, P.A. (2001). Ship structural safety and reliability, *Progress in Structural Engineering and Materials*, 3: 198-210.
26. PAIK, J.K. & KIM, D.K. (2012). Advanced method for the development of an empirical model to predict time-dependent corrosion wastage, *Corrosion Science*, 63: 51-58.
27. PAIK, J.K., KIM, K.J., LEE, J.H., JUNG, B.G. & KIM, S.J. (2017). Test database of the mechanical properties of mild, high-tensile and stainless steel and aluminium alloy associated with cold temperatures and strain rates, *Ships and Offshore Structures*, 12(sup1): 1-27.
28. PAIK, J.K., KIM, B.J., SOHN, J.M., KIM, S.H., JEONG, J.M. & PARK, J.S. (2012). On buckling collapse of a fusion-welded aluminium stiffened plate structure: An experimental and numerical study, *Journal of Offshore Mechanics and Arctic Engineering*, 134: 021402.1-8.
29. PAIK, J.K., LEE, J.M., HWANG, J.S. & PARK, Y.I. (2003a). A time-dependent corrosion wastage model for the structures of single- and double-hull tankers and FSOs and FPSOs, *Marine Technology*, 40(3): 201-217.
30. Paik, J.K., & Melchers, R.E. (2008). *Condition Assessment of Aged Structures*. CRC Press, New York.
30. PAIK, J.K. & PEDERSEN, P.T. (1996). A simplified method for predicting the ultimate compressive strength of ship panels, *International Shipbuilding Progress*, 43: 139-157.
31. PAIK, J.K. & THAYAMBALLI, A.K. (2007). *Ship-Shaped Offshore Installations: Design, Building, and Operation*. Cambridge University Press, Cambridge.
32. PAIK, J.K., THAYAMBALLI, A.K., PARK, Y.I. & HWANG, J.S. (2003b). A time-dependent corrosion wastage model for bulk carrier structures, *International Journal of Maritime Engineering*, 145(A2): 61-87.
33. PAIK, J.K., THAYAMBALLI, A.K., RYU, J.Y., JANG, J.H., SEO, J.K., PARK, S.W., SEO, S.K., ANDRIEU, C., COJEEN, H.P. & KIM, N.I. (2006). The statistics of weld induced initial imperfections in aluminium stiffened plate structures for marine applications, *International Journal of Maritime Engineering*, 148(Part A1): 19-63.
34. PAIK, J.K. & YI, M.S. (2006). *Experimental and Numerical Investigations of Welding-Induced Distortions and Stresses in Steel Stiffened Plate Structures*. The Korea Ship and

- Offshore Research Institute, Pusan National University, Busan, South Korea.
35. SMITH, C.S., DAVIDSON, P.C., CHAPMAN, J.C. & DOWLING, P.J. (1988). Strength and stiffness of ships' plating under in-plane compression and tension, *Transactions of the Royal Institution of Naval Architects*, 130: 277-296.
  36. TERESA, M. & CRAIG, F. (2013). Effect of weld-induced imperfections on the ultimate strength of an aluminium patrol boat determined by the ISFEM rapid assessment method, *Ships and Offshore Structures*, 9(2): 218-235.
  37. UEDA, Y. (1999). *Computational Welding Mechanics (A volume of selected papers in the commemoration of the retirement from Osaka University)*. Joining and Welding Research Institute, Osaka University, Osaka, Japan.
  38. VHANMANE, S. & BHATTACHARYA, B. (2008). Estimation of ultimate hull girder strength with initial imperfections, *Ships and Offshore Structures*, 3(3): 149-158.
  39. WANG, J., HAN, J., DOMBLESKY, J.P., LI, W., YANG, Z. & ZHAO, Y. (2015), Predicting distortion in butt welded plates using an equivalent plane stress representation based on inherent shrinkage volume, *Journal of Manufacturing Science and Engineering*, 138(1): 011012.
  40. WOO, W.C., KIM, D.G. & AN, G.B. (2015). Residual stress measurements using neutron diffraction, *Journal of Welding and Joining*, 33(1): 30-34 (in Korean).
  41. Xstress 3000 Manual (2010). Stresstech Inc., Finland.
  42. YI, M.S., HYUN, C.M. & PAIK, J.K. (2018). Three-dimensional thermo-elastic-plastic finite element method modeling for predicting weld-Induced residual stresses and distortions in steel stiffened-plate structures, *World Journal of Engineering and Technology*, 6: 176-200.